Flutter and Forced Response of Mistuned Rotors Using Standing Wave Analysis

John Dugundji* and David J. Bundas†
Massachusetts Institute of Technology, Cambridge, Massachusetts

The flutter and forced response of a tuned and mistuned rotor is examined using a standing wave approach rather than the traditional traveling wave analysis. This approach uses standing wave modes to obtain the equations of motion of the entire rotor, together with Whitehead's incompressible aerodynamic cascade theory, rewritten for arbitrary transient motion by fitting the sinusoidal aerodynamic coefficients of Whitehead by Padé approximants. The resulting equations of motion are written in the standard matrix form, $M\ddot{x}+C\dot{x}+Kx=F(t)$, where M,C,K are all real coefficients. Applications are given for vibration modes, flutter, and forced response. The present procedure represents an alternate approach to the hitherto traditional traveling wave analysis of rotor flutter. These standing wave methods may prove to be more versatile in dealing with certain applications such as mistuned rotors, "localized" blade flutter, low engine order excitation, transient impulses on the rotor, and coupling in with forced response and dynamic shaft problems.

Introduction

MOST work involving the aeroelastic stability of rotors makes use of cascade aerodynamic models that assume that the blade motions are represented by sinusoidal traveling waves moving around the circumference; see, e.g., Carta,[1] Snyder and Commerford,[2] and Mikolajczak et al.[3] This traveling wave approach is a natural choice, since the flutter mode of (tuned) rotors appears as a traveling wave.

In contrast to this traveling wave approach, conventional flutter analyses of aircraft wings utilize the coupling together of standing wave modes. Standing waves may also be used in the analysis of rotors, since it is the presence of aerodynamic and gyroscopic forces that changes the original nonrotating, vacuum, standing wave rotor modes into traveling wave flutter modes. In an earlier report, Dugundji[4] reviewed in a general way the relations between rotor traveling wave flutter analyses and standing wave methods. Although both are equivalent, these standing wave methods may prove to be more versatile in dealing with certain applications such as coupling in with forced response and dynamic shaft problems, transient impulses on the rotor, and mistuned rotors.

The present article applies these standing wave analysis methods to the flutter and forced response of tuned and mistuned rotors. First the rotor equations are expressed in terms of standing wave modes, then the sinusoidal motion traveling wave flutter forces are recast in standing wave form, then finally some applications are made to tuned and mistuned rotor systems. Further details of the present article can be found in Ref. 5.

Standing Wave Representation of Rotor

Consider a mistuned rotor with N blades mounted on a heavy, rigid disk as shown in Fig. 1. Each blade is located at an angle $\theta_j=(2\pi/N)j$ along the circumference, and may have a slightly different mass and stiffness from its neighbor. For simplicity, only a single torsion degree of freedom α_j will be considered for each blade.

The sinusoidal motion of the N blades α_j can be characterized by the superposition of N traveling wave modes as,

$$\alpha_j=\sum_{r=0}^{N-1}(a_{rR}+ia_{rI})\exp[i(\omega t+j\beta_r)] \tag{1}$$

where $\beta_r=r2\pi/N$ represents the interblade phase angle for the rth traveling wave. Since there are N modes, this requires a total of $2N$ constants (a_{rR}, a_{rI}) to characterize any sinusoidal motion of the N blades (N amplitudes, N phases). Such an approach was used by Srinivasan[6] and Kaza and Kielb[7] to characterize mistuned rotors. For tuned rotors, each traveling wave mode r can be investigated separately, so that the summation sign can be omitted in Eq. (1).

Alternatively, the arbitrary motion of the N blades α_j can also be characterized by superposition of N standing wave modes as,

$$\alpha_j=\sum_{r=0}^{(N-1)/2}[\alpha_{cr}(t)\cos j\beta_r+\alpha_{sr}(t)\sin j\beta_r] \tag{2}$$

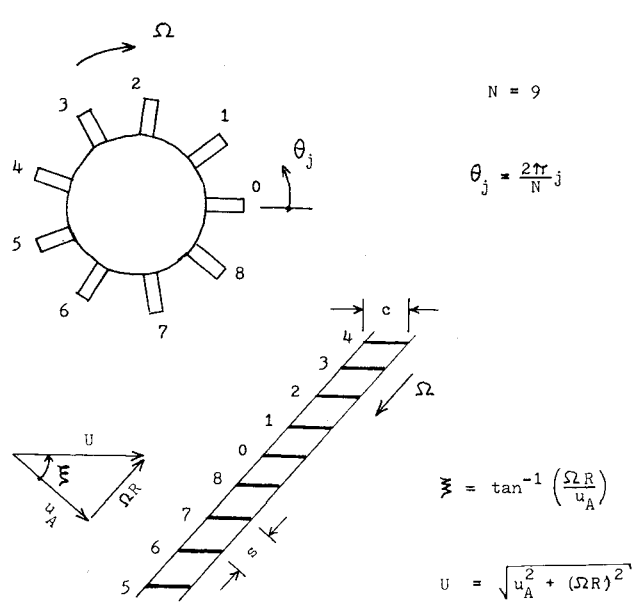

Fig. 1 Rotor layout and geometry.

Received April 27, 1983; presented as Paper 83-0845 at the AIAA/ASME/ASCE/AHS 24th Structures, Structural Dynamics and Materials Conference, Lake Tahoe, Nev., May 2-4, 1983; revision received Jan. 9, 1984.

*Professor, Department of Aeronautics and Astronautics. Member AIAA.

†Research Assistant, Department of Aeronautics and Astronautics.

where $\alpha_{cr}(t)$ and $\alpha_{sr}(t)$ now represent a total of N generalized coordinates. (Note: N is here assumed to be an odd number of blades. For N=even, an additional mode would be required in the above.) If further, one assumes sinusoidal motion $\alpha_{cr}(t)=(\alpha_{crR}+i\alpha_{crI})e^{i\omega t}$, $\alpha_{sr}(t)=(\alpha_{srR}+i\alpha_{srI})e^{i\omega t}$, one can relate the $2N$ standing wave coefficients α_{crR}, α_{crI},... to the $2N$ traveling wave coefficients a_{rR}, a_{rI} by trigonometric expansion.

The standing wave representation, Eq. (2), is useful since it allows for arbitrary transient motion of the blades rather than only sinusoidal motion. It can be rewritten in convenient matrix form as,

$$\boldsymbol{\alpha}=\boldsymbol{P}\boldsymbol{q} \tag{3}$$

where

$$\boldsymbol{\alpha}=\begin{Bmatrix}\alpha_0\\ \alpha_1\\ \alpha_2\\ \vdots\\ \alpha_{N-1}\end{Bmatrix},\quad \boldsymbol{q}=\begin{Bmatrix}\alpha_{C0}\\ \alpha_{C1}\\ \alpha_{S1}\\ \vdots\\ \alpha_{S[(N-1)/2]}\end{Bmatrix},\quad \beta_r=\frac{2\pi}{N}r \tag{4}$$

$$\boldsymbol{P}=\begin{bmatrix} 1 & \cos 0\beta_1 & \sin 0\beta_1 & \cdots \sin 0\beta_{(N-1)/2}\\ 1 & \cos 1\alpha_1 & \sin 1\beta_1 & \cdots \sin 1\beta_{(N-1)/2}\\ \vdots & \vdots & \vdots & \vdots\\ 1 & \cos(N-1)\beta_1 & \sin(N-1)\beta_1 & \cdots \sin(N-1)\beta_{(N-1)/2}\end{bmatrix}$$

The generalized coordinates q appearing above and in Eq. (2) are sometimes referred to as "multiblade coordinates"; see, for example, Hohenemser and Yin.[8] Also, one can show the important properties of the $\boldsymbol{P}$ matrix,

$$\boldsymbol{P}^T\boldsymbol{P}=\boldsymbol{D}=\begin{bmatrix} N & & & & 0\\ & N/2 & & & \\ & & N/2 & & \\ & & & N/2 & \\ 0 & & & & \ddots\end{bmatrix} \tag{5}$$

$$\boldsymbol{P}^{-1}=\boldsymbol{D}^{-1}\boldsymbol{P}^T$$

which come from applying the trigonometric identities,

$$\begin{aligned}\cos n\theta_j\cos r\theta_j &= \tfrac{1}{2}\cos(n-r)\theta_j+\tfrac{1}{2}\cos(n+r)\theta_j\\ \sin n\theta_j\sin r\theta_j &= \tfrac{1}{2}\cos(n-r)\theta_j-\tfrac{1}{2}\cos(n+r)\theta_j\\ \sin n\theta_j\cos r\theta_j &= \tfrac{1}{2}\sin(n-r)\theta_j+\tfrac{1}{2}\sin(n+r)\theta_j\end{aligned} \tag{6}$$

$$\sum_{j=0}^{N-1}\sin m\theta_j=0$$

$$\sum_{j=0}^{N-1}\cos m\theta_j=\begin{cases}N & \text{for } m=0,\ N,\ 2N,\ldots\\ 0 & \text{otherwise}\end{cases}$$

The equations of motion for the twist α_j of each blade of the rotor shown in Fig. 1 can be written in matrix form as,

$$[\,I_\alpha\,]\ddot{\boldsymbol{\alpha}}+[\,c_s\,]\dot{\boldsymbol{\alpha}}+[\,k_\alpha\,]\boldsymbol{\alpha}=\boldsymbol{m}_\alpha \tag{7}$$

where I_α, c_s, k_α are the moment of inertia, structural damping, and stiffness, and $\boldsymbol{m}_\alpha$ is the moment applied to each blade. Since the blades are mounted on a rigid disk, the I_α, c_s, k_α are all diagonal matrices, and only aerodynamic coupling through $\boldsymbol{m}_\alpha$ is possible between the blades. Introducing Eq. (3) into Eq. (7) and multiplying by $\boldsymbol{P}^T$ gives the standing wave representation of the rotor as,

$$\boldsymbol{M}\ddot{\boldsymbol{q}}+\boldsymbol{C}\dot{\boldsymbol{q}}+\boldsymbol{K}\boldsymbol{q}=\boldsymbol{P}^T\boldsymbol{m}_\alpha \tag{8}$$

where

$$\boldsymbol{M}=\boldsymbol{P}^T\boldsymbol{I}_\alpha\boldsymbol{P},\quad \boldsymbol{C}=\boldsymbol{P}^T\boldsymbol{c}_s\boldsymbol{P},\quad \boldsymbol{K}=\boldsymbol{P}^T\boldsymbol{k}_\alpha\boldsymbol{P} \tag{9}$$

Equation (8) generally represents N coupled equations for the motion of the N blades. For tuned rotors, where all blades are equal, Eq. (8) again reduces to N uncoupled equations because of the $\boldsymbol{P}$ matrix properties given by Eq. (5).

Transient Cascade Air Forces

To complete the standing wave formulation, the sinusoidal traveling wave cascade air forces must also be recast into arbitrary motion, standing wave form. The present formulation follows that originally laid out in Ref. 4. Given a traveling wave deflection of amplitude $\bar{\alpha}$ and the corresponding traveling wave air forces (aerodynamic moment here),

$$\alpha_j=\bar{\alpha}\exp[\,i(\omega t+j\beta_r)\,] \tag{10}$$

$$m_{\alpha j}=2\pi\rho U^2b^2(A_R+iA_I)\bar{\alpha}\exp[\,i(\omega t+j\beta_r)\,] \tag{11}$$

In the above ρ, U, b represent the air density, velocity and semichord, respectively. Equations (10) and (11) can be represented physically by taking their real parts as,

$$\alpha_j=\bar{\alpha}[\cos\omega t\,\cos j\beta_r-\sin\omega t\,\sin j\beta_r] \tag{12}$$

$$\begin{aligned}m_{\alpha j}=2\pi\rho U^2b^2\bar{\alpha}\{&[A_R\cos\omega t-A_I\sin\omega t]\cos j\beta_r\\ &+[-A_I\cos\omega t-A_R\sin\omega t]\sin j\beta_r\}\end{aligned} \tag{13}$$

Then by adding two traveling waves of amplitude $\bar{\alpha}/2$ traveling in opposite directions ($+\beta_r$ and $-\beta_r$), and their corresponding air forces, one obtains,

$$\alpha_j=\bar{\alpha}\cos\omega t\,\cos j\beta_r \tag{14}$$

$$\begin{aligned}m_{\alpha j}=2\pi\rho U^2b^2\{&[\bar{A}_R\bar{\alpha}\cos\omega t-\bar{A}_I\sin\omega t]\cos j\beta_r\\ &+[-\bar{\bar{A}}_I\bar{\alpha}\cos\omega t-\bar{\bar{A}}_R\bar{\alpha}\sin\omega t]\sin j\beta_r\}\end{aligned} \tag{15}$$

where the coefficients $\bar{A}_R, \bar{A}_I, \bar{\bar{A}}_R, \bar{\bar{A}}_I$ are related to one half the sums and differences of the traveling wave coefficients $A_R^+, A_I^+, A_R^-, A_I^-$ by,

$$\begin{aligned}\bar{A}_R&=(A_R^+ +A_R^-)/2, & \bar{A}_I&=(A_I^+ +A_I^-)/2\\ \bar{\bar{A}}_R&=(A_R^+ -A_R^-)/2, & \bar{\bar{A}}_I&=(A_I^+ -A_I^-)/2\end{aligned} \tag{16}$$

One can rewrite Eqs. (14) and (15) in terms of an arbitrary function of time $\alpha_c(t)$ as,

$$\alpha_j=\alpha_c(t)\cos j\beta_r \tag{17}$$

$$m_{\alpha j}=2\pi\rho U^2b^2\left\{\left[B_1\frac{b}{U}\dot{\alpha}_c+B_0\alpha_c\right]\cos j\beta_r+\left[\bar{B}_1\frac{b}{U}\dot{\alpha}_c+\bar{B}_0\alpha_c\right]\sin j\beta_r\right\} \tag{18}$$

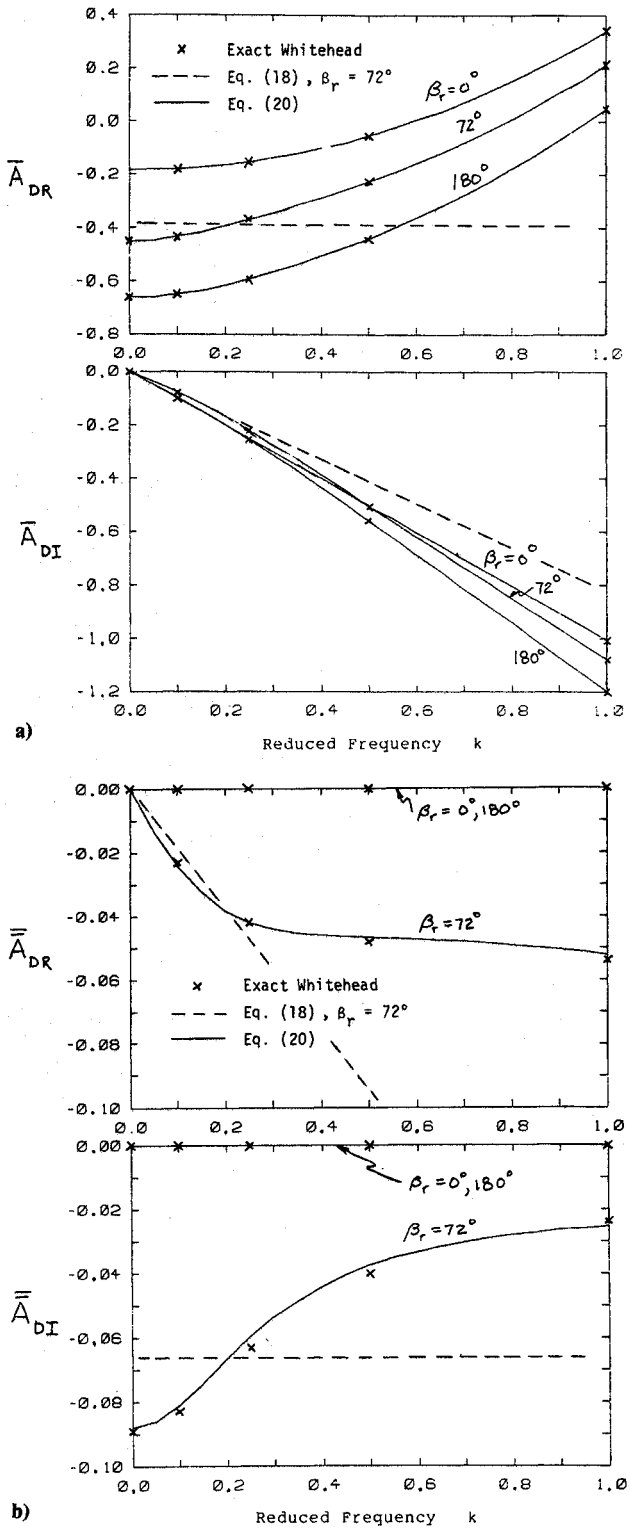

Fig. 2 Fitting of Whitehead coefficients. Type A_D, $\xi = 45$ deg, $s/c = 1$, $\eta = 0$.

since if one substitutes $\alpha_c = \bar{\alpha}\cos\omega t$ into the above, one will obtain Eqs. (14) and (15) again, where now the new constants $B_1, B_0, \tilde{B}_1, \tilde{B}_0$ are related to the traveling wave coefficients through the relations,

$$B_0 = \bar{A}_R, \qquad \tilde{B}_0 = -\bar{\bar{A}}_I$$
$$kB_1 = \bar{A}_I, \qquad k\tilde{B}_1 = \bar{\bar{A}}_R \tag{19}$$

The coefficients $\bar{A}_R, \bar{A}_I, \bar{\bar{A}}_R, \bar{\bar{A}}_I$ are generally functions of reduced frequencies $k = \omega b/U$, and are shown plotted in Fig. 2, for the incompressible, two-dimensional theory of Whitehead.[9] Using Eq. (19), one picks $B_0, B_1, \tilde{B}_0, \tilde{B}_1$ to obtain a fit of the traveling wave data of Fig. 2. Unfortunately, it can be seen from Fig. 2 that the B_i coefficients give poor fits to the traveling wave data over the frequency range $k = 0$ to $k = 1.0$ of interest here.

To obtain a better fit, a more general approximation is used in place of Eq. (18), namely,

$$m_{\alpha j} = 2\pi\rho U^2 b^2 \left\{ \left[B_2 \frac{b^2}{U^2}\ddot{\alpha}_c + B_1 \frac{b}{U}\dot{\alpha}_c + B_0\alpha_c + G_1 Y_c \right] \cos j\beta_r \right.$$
$$\left. + \left[\tilde{B}_2 \frac{b^2}{U^2}\ddot{\alpha}_c + \tilde{B}_1 \frac{b}{U}\dot{\alpha}_c + \tilde{B}_0\alpha_c + \tilde{G}_1 Y_c \right] \sin j\beta_r \right\} \tag{20}$$

$$\frac{b}{U}\dot{Y}_c + g_0 Y_c = \frac{b}{U}\dot{\alpha}_c \tag{21}$$

The above formulation is motivated by the isolated airfoil (Theodorsen) air forces, and is more familiar if one takes the Laplace transform

$$\int_0^\infty f(t)e^{-pt}\,dt$$

of these equations to obtain,

$$m_{\alpha j} = 2\pi\rho U^2 b^2 \{ [B_2\tilde{p}^2 + B_1\tilde{p} + B_0 + G_1\tilde{p}/(\tilde{p}+g_0)]\bar{\alpha}\cos j\beta_r$$
$$+ [\tilde{B}_2\tilde{p}^2 + \tilde{B}_1\tilde{p} + \tilde{B}_0 + \tilde{G}_1\tilde{p}/(\tilde{p}+g_0)]\bar{\alpha}\sin j\beta_r \} \tag{22}$$

where $\tilde{p} = pb/U$, and the augmented state variable Y_c in Eq. (20) has been replaced by its solution from Eq. (21). Substituting $\alpha_c = \bar{\alpha}\cos\omega t$ and $Y_c = Y_{cc}\cos\omega t + Y_{cs}\sin\omega t$ into Eq. (21), solving Y_{cc} and Y_{cs}, then placing into Eq. (20) and comparing terms $\cos\omega t\cos j\beta_r$, $\sin\omega t\cos j\beta_r$, etc., with Eq. (15) gives now the more versatile relations,

$$-k^2B_2 + B_0 + k^2G_1/(k^2+g_0^2) = \bar{A}_R$$
$$kB_1 + kg_0G_1/(k^2+g_0^2) = \bar{A}_I$$
$$-k^2\tilde{B}_2 + \tilde{B}_0 + k^2\tilde{G}_1/(k^2+g_0^2) = -\bar{\bar{A}}_I \tag{23}$$
$$k\tilde{B}_1 + kg_0\tilde{G}_1/(k^2+g_0^2) = \bar{\bar{A}}_R$$

Using the above relations, one can now choose the nondimensional coefficients $B_2, B_1, B_0, G_1, g_0, \tilde{B}_2, \tilde{B}_1, \tilde{B}_0, \tilde{G}_1$ to obtain a good fit of the traveling wave data over the range $k = 0$ to $k = 1$ of interest here (see Fig. 2). To solve for these coefficients from Eq. (23), the traveling wave data were simply fit at $k = 0$, $k = 0.1$, and $k = 1$, respectively. Also the g_0 obtained from the first two equations was made equal to that from the last two, in order to avoid introducing an additional augmented state variable $\tilde{Y}_c$ in Eq. (20).

The air force representation given by Eqs. (20) and (21) using augmented states Y_c is a popular one for fixed-wing aircraft, particularly when control system interactions are investigated. They are also referred to as Padé approximants and were used by Vepa[10] and Edwards et al.[11] for fixed-wing aircraft.

The corresponding air force representation for the $\alpha_j = \alpha_c(t)\sin j\beta_r$ standing wave mode can similarly be obtained by subtracting two traveling waves of amplitude $\bar{\alpha}/2$ traveling in opposite directions to obtain $\alpha_j = \bar{\alpha}\sin\omega t\sin j\beta_r$, then following through as before. Summarizing, the deflections and corresponding air forces for arbitrary transient motion of a cascade in a *standing wave* deflection pattern can be represented as,

$$\alpha_j = \alpha_c(t)\cos j\beta_r + \alpha_s(t)\sin j\beta_r \tag{24}$$

$$m_{\alpha j}=2\pi\rho U^2 b^2\{[B_2\sigma^2\ddot{\alpha}_c+B_1\sigma\dot{\alpha}_c+B_0\alpha_c+G_1 Y_c$$
$$-\tilde{B}_2\sigma^2\ddot{\alpha}_s-\tilde{B}_1\sigma\dot{\alpha}_s-\tilde{B}_0\alpha_s-\tilde{G}_1 Y_s]\cos j\beta_r$$
$$+[B_2\sigma^2\ddot{\alpha}_s+B_1\sigma\dot{\alpha}_s+B_0\alpha_s+G_1 Y_s$$
$$+\tilde{B}_2\sigma^2\ddot{\alpha}_c+\tilde{B}_1\sigma\dot{\alpha}_c+\tilde{B}_0\alpha_c+\tilde{G}_1 Y_c]\sin j\beta_r\} \quad (25)$$

$$\sigma\dot{Y}_c+g_0 Y_c=\sigma\dot{\alpha}_c \quad (26)$$

$$\sigma\dot{Y}_s+g_0 Y_s=\sigma\dot{\alpha}_s \quad (27)$$

where $B_2,B_1,B_0,\ldots$ are constants found by fitting the sinusoidal traveling wave coefficients A_R and A_I as indicated by Eqs. (23) and (16), and $\sigma\equiv b/U$ for convenience in writing.

The preceding procedure can be extended to both bending and torsion motions of a cascade by writing

$$\begin{Bmatrix} h_j/b \\ \alpha_j \end{Bmatrix}=\begin{Bmatrix} \bar{h}/b \\ \bar{\alpha} \end{Bmatrix}\exp[i(\omega t+j\beta_r)] \quad (28)$$

$$\begin{Bmatrix} \ell_j \\ m_{\alpha j}/b \end{Bmatrix}=2\pi\rho U^2 b\begin{bmatrix} A_A & A_B \\ A_C & A_D \end{bmatrix}\begin{Bmatrix} \bar{h}/b \\ \bar{\alpha} \end{Bmatrix}\exp[i(\omega t+j\beta_r)] \quad (29)$$

where $A_A,A_B,\ldots$ are nondimensional coefficients for the air forces. As in Ref. 9, the rotations and moments are taken about the leading edge. See Fig. 3 for notation and positive directions. These complex coefficients are related to the Whitehead coefficients by,

$$A_A=ikC_{Fq},\quad A_B=-C_{F\alpha},\quad A_C=-2ikC_{Mq},\quad A_D=2C_{M\alpha} \quad (30)$$

For arbitrary transient motions, one can write additional expressions similar to Eqs. (24-27) as follows:

$$h_j=h_c(t)\cos j\beta_r+h_s(t)\sin j\beta_r$$

$$\ell_j=2\pi\rho U^2 b\left\{\left[B_{2A}\sigma^2\frac{\ddot{h}_c}{b}+B_{1A}\sigma\frac{\dot{h}_c}{b}+\ldots\right\}\right.$$

$$m_{\alpha j}/b=2\pi\rho U^2 b\left\{\left[B_{2C}\sigma^2\frac{\ddot{h}_c}{b}+B_{1C}\sigma\frac{\dot{h}_c}{b}+\ldots\right\}\right.$$

$$\sigma\dot{Y}_{hc}+g_0 Y_{hc}=\sigma(\dot{h}_c/b),\quad \sigma\dot{Y}_{hs}+g_0 Y_{hs}=\sigma(\dot{h}_s/b) \quad (31)$$

where now one distinguishes between $B_{iA},B_{iB},B_{iC},B_{iD}$, etc., depending on the type of motion and force. The constant coefficients B_{iA},B_{iB}, etc., are given in Tables 1 and 2 for Whitehead's two-dimensional cascade theory for a gap-chord ratio $s/c=1$, stagger ratios $\xi=0$ and 45 deg, and for rotations and moments about the leading edge. To transfer to any other rotation point (elastic axis), one can develop the simple relations from Fig. 3, namely,

$$(A_A)_\eta=(A_A)_0$$
$$(A_B)_\eta=(A_B)_0+2\eta(A_A)_0$$
$$(A_C)_\eta=(A_C)_0+2\eta(A_A)_0$$
$$(A_D)_\eta=(A_D)_0+2\eta[(A_C)_0+(A_B)_0]+4\eta^2(A_A)_0 \quad (32)$$

The seemingly cumbersome algebraic expressions given by Eqs. (24-27) can be combined with the previous standing wave representation of the rotor considered earlier to give a convenient and compact matrix form for the air forces, namely,

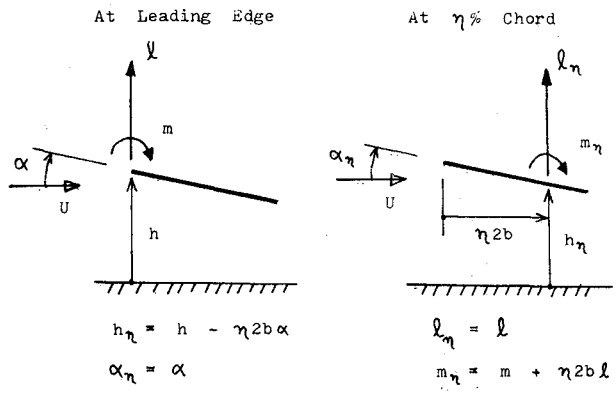

Fig. 3 Force notation and axis transfer.

$$\alpha=Pq \quad (33)$$

$$m_\alpha=2\pi\rho U^2 b^2 P(B_2\sigma^2\ddot{q}+B_1\sigma\dot{q}+B_0 q+G_1 Y) \quad (34)$$

$$\sigma\dot{Y}+g_0 Y=\sigma\dot{q} \quad (35)$$

where the α, q, and P matrices have been defined previously in Eqs. (3) and (4), and one has additionally,

$$B_2=\begin{array}{c} \begin{matrix} r=0 & & r=1 & & & r=\frac{N-1}{2} \end{matrix} \\ \begin{bmatrix} B_{2D} & 0 & 0 & 0 & 0 & 0 & 0 \\ 0 & B_{2D} & -\tilde{B}_{2D} & 0 & 0 & 0 & 0 \\ 0 & \tilde{B}_{2D} & B_{2D} & 0 & 0 & & \\ 0 & 0 & 0 & & & \vdots & \vdots \\ \vdots & & & & & B_{2D} & -\tilde{B}_{2D} \\ & & & & & \tilde{B}_{2D} & B_{2D} \end{bmatrix} \end{array} ,B_1,B_0,G_1=\text{etc.}$$

$$g_0=\begin{array}{c} \begin{matrix} r=0 & r=1 & & r=\frac{N-1}{2} \end{matrix} \\ \begin{bmatrix} g_0 & & & \\ & g_0 & & \\ & & g_0 & \\ & & & \ddots \\ & & & g_0 \\ & & & & g_0 \end{bmatrix} \end{array}$$

$$Y=\begin{bmatrix} Y_{C0} \\ Y_{C1} \\ Y_{S1} \\ \vdots \\ Y_S\left(\frac{N-1}{2}\right) \end{bmatrix} \quad (36)$$

where the elements making up the B_2,B_1, etc., matrices are taken from Tables 1 and 2 for the appropriate mode r, i.e., $\beta_r=2\pi r/N$. Note the antisymmetric coupling of these

Table 1 Transient Whitehead coefficients, $\xi = 0$ deg, $s/c = 1$, $\eta = 0$

β_r, deg	Type	B_2	B_1	B_0	G_1	g_0	$\tilde{B}_2$	$\tilde{B}_1$	$\tilde{B}_0$	$\tilde{G}_1$
0	A	−0.366	−0.305	0.000	0.000	0.000	0.000	0.000	0.000	0.000
	B	0.366	0.860	0.305	0.000	0.000	0.000	0.000	0.000	0.000
	C	0.366	0.110	0.000	0.000	0.000	0.000	0.000	0.000	0.000
	D	−0.432	−0.788	−0.110	0.000	0.000	0.000	0.000	0.000	0.000
36	A	−0.435	−0.410	0.000	−0.055	0.140	0.000	0.000	0.000	0.000
	B	0.435	1.068	0.800	−0.303	0.140	0.000	0.000	0.000	0.000
	C	0.435	0.184	0.000	0.025	0.140	0.000	0.000	0.000	0.000
	D	−0.498	−0.964	−0.360	0.138	0.140	0.000	0.000	0.000	0.000
72	A	−0.496	−0.510	0.000	−0.116	0.235	0.000	0.000	0.000	0.000
	B	0.496	1.258	1.005	−0.319	0.235	0.000	0.000	0.000	0.000
	C	0.496	0.256	0.000	0.059	0.235	0.000	0.000	0.000	0.000
	D	−0.560	−1.128	−0.506	0.162	0.235	0.000	0.000	0.000	0.000
108	A	−0.545	−0.590	0.000	−0.175	0.300	0.000	0.000	0.000	0.000
	B	0.545	1.410	1.173	−0.327	0.300	0.000	0.000	0.000	0.000
	C	0.545	0.316	0.000	0.094	0.300	0.000	0.000	0.000	0.000
	D	−0.610	−1.262	−0.628	0.174	0.300	0.000	0.000	0.000	0.000
144	A	−0.575	−0.643	0.000	−0.214	0.335	0.000	0.000	0.000	0.000
	B	0.575	1.506	1.283	−0.328	0.335	0.000	0.000	0.000	0.000
	C	0.575	0.354	0.000	0.118	0.335	0.000	0.000	0.000	0.000
	D	−0.638	−1.348	−0.706	0.182	0.335	0.000	0.000	0.000	0.000
180	A	−0.586	−0.661	0.000	−0.231	0.350	0.000	0.000	0.000	0.000
	B	0.586	1.540	1.321	−0.329	0.350	0.000	0.000	0.000	0.000
	C	0.586	0.366	0.000	0.129	0.350	0.000	0.000	0.000	0.000
	D	−0.648	−1.378	−0.734	0.186	0.350	0.000	0.000	0.000	0.000

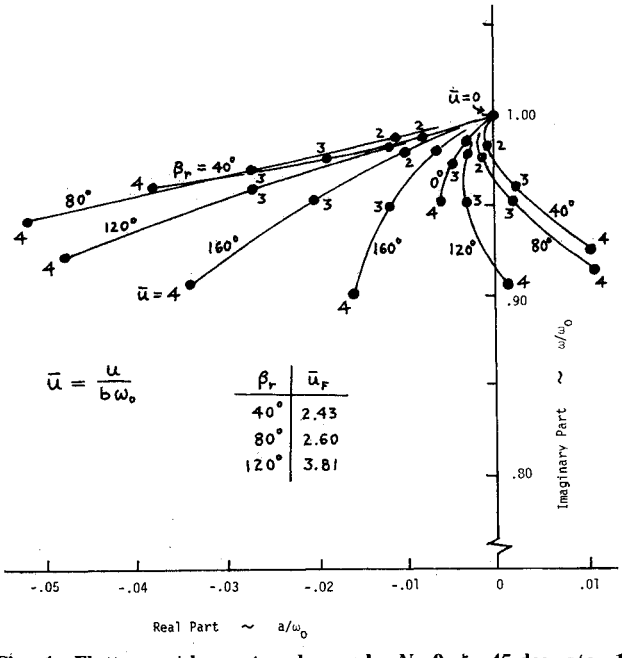

Fig. 4 Flutter root locus: tuned cascade. $N = 9$, $\xi = 45$ deg, $s/c = 1$, $\eta = 0.5$, $v_0 = 86.2$, $\zeta_i = 0$.

matrices through the $\tilde{B}_{ID}$ terms. Similar convenient matrix forms can be developed for the combined bending-torsion air forces. See Ref. 5. Equations (33-35) constitute a convenient arbitrary transient motion, standing wave representation of the air forces which can be readily combined with the previous dynamic equations for the rotor, Eq. (8).

For interest, the appropriate coefficients B_2, B_1, B_0, G_1, g_0 were also fitted for the isolated airfoil (Theodorsen) air forces and are given in Table 3 for the rotation and moment about the leading edge ($\eta = 0$, or equivalently $a = -1$). These forces can be expressed by setting $\beta_r = 0$ in the previous equations to give

$$\ell = 2\pi\rho U^2 b\left\{B_{2A}\sigma^2\frac{\ddot{h}}{b} + B_{1A}\sigma\frac{\dot{h}}{b} + B_{0A}\frac{h}{b} + G_{1A}Y_h + B_{2B}\sigma^2\ddot{\alpha} + B_{1B}\sigma\dot{\alpha} + B_{0B}\alpha + G_{1B}Y_\alpha\right\}$$

$$m_\alpha/b = 2\pi\rho U^2 b\left\{B_{2C}\sigma^2\frac{\ddot{h}}{b} + B_{1C}\sigma\frac{\dot{h}}{b} + B_{0C}\frac{h}{b} + G_{1C}Y_h + B_{2D}\sigma^2\ddot{\alpha} + B_{1D}\sigma\dot{\alpha} + B_{0D}\alpha + G_{1D}Y_\alpha\right\} \tag{37}$$

$$\sigma\dot{Y}_h + g_0 Y_h = \sigma(\dot{h}/b), \qquad \sigma\dot{Y}_\alpha + g_0 Y_\alpha = \sigma\dot{\alpha} \tag{38}$$

The fit on these coefficients, although adequate, was not quite as good as for the Whitehead cascade air forces. For better accuracy, an additional $G_2 Y_2$ term and an additional g_0 should be included in the Padé approximants here (this would be equivalent to using the Jones approximation of the Theodorsen function[12]). In a recent related study, Rock and DeBra[13] have shown that when wind tunnel walls are present, the air forces in incompressible flow can be adequately represented by a single $G_1 Y$ term as in Eqs. (37) and (38).

Application to Vibration Modes

To obtain the vibration modes of the rotor, one goes back to the standing wave representation given by Eqs. (3) and (8), and sets all damping forces C and applied moments m_α equal to zero to obtain

$$M\ddot{q} + Kq = 0 \tag{39}$$

where the M and K matrices are given by Eq. (9). Then, setting $q = \tilde{q}e^{i\omega t}$, these equations can be readily solved for the natural frequencies ω and mode shapes $\tilde{q}$ by standard methods.

Table 2 Transient Whitehead coefficients, $\xi = 45$ deg, $s/c = 1$, $\eta = 0$

β_r, deg	Type	B_2	B_1	B_0	G_1	g_0	$\tilde{B}_2$	$\tilde{B}_1$	$\tilde{B}_0$	$\tilde{G}_1$
0	A	−0.455	−0.427	0.000	0.000	0.000	0.000	0.000	0.000	0.000
	B	0.455	1.119	0.427	0.000	0.000	0.000	0.000	0.000	0.000
	C	0.455	0.182	0.000	0.000	0.000	0.000	0.000	0.000	0.000
	D	−0.524	−1.008	−0.184	0.000	0.000	0.000	0.000	0.000	0.000
36	A	−0.471	−0.445	0.000	−0.038	0.175	0.000	−0.010	0.000	0.067
	B	0.471	1.159	0.660	−0.156	0.175	0.000	−0.013	−0.370	0.275
	C	0.471	0.202	0.000	0.021	0.175	0.000	0.034	0.000	−0.034
	D	−0.534	−1.044	−0.322	0.090	0.175	0.000	−0.026	0.128	−0.116
72	A	−0.493	−0.493	0.000	−0.110	0.295	0.000	−0.014	0.000	0.095
	B	0.493	1.236	0.867	−0.216	0.295	0.000	−0.018	−0.308	0.176
	C	0.493	0.242	0.000	0.062	0.295	0.000	0.048	0.000	−0.048
	D	−0.556	−1.112	−0.452	0.118	0.295	0.000	−0.034	0.088	−0.068
108	A	−0.517	−0.541	0.000	−0.188	0.375	0.000	−0.014	0.000	0.089
	B	0.517	1.314	1.041	−0.234	0.375	0.000	−0.015	−0.222	0.095
	C	0.517	0.282	0.000	0.105	0.375	0.000	0.045	0.000	−0.045
	D	−0.580	−1.180	−0.562	0.128	0.375	0.000	−0.030	0.054	−0.036
144	A	−0.536	−0.571	0.000	−0.247	0.420	0.000	−0.007	0.000	0.052
	B	0.536	1.368	1.158	−0.234	0.420	0.000	−0.008	−0.116	0.040
	C	0.536	0.312	0.000	0.136	0.420	0.000	0.025	0.000	−0.025
	D	−0.596	−1.230	−0.636	0.128	0.420	0.000	−0.018	0.026	−0.014
180	A	−0.542	−0.582	0.000	−0.268	0.435	0.000	0.000	0.000	0.000
	B	0.542	1.387	1.198	−0.234	0.435	0.000	0.000	0.000	0.000
	C	0.542	0.322	0.000	0.148	0.435	0.000	0.000	0.000	0.000
	D	−0.602	−1.246	−0.662	0.128	0.435	0.000	0.000	0.000	0.000

Table 3 Transient Theodorsen coefficients, $\eta = 0.0$
Moments taken about the leading edge, $\eta = 0.0$, or $a = -1$

Type	B_2	B_1	B_0	G_1	g_0
A	−0.470	−0.526	0.000	−0.072	0.130
B	0.565	1.229	1.000	−0.244	0.130
C	0.485	0.263	0.000	0.036	0.130
D	−0.595	−1.114	−0.500	0.122	0.130

For the tuned rotor case, where all blades are identical, Eq. (39) will reduce to N uncoupled equations because of the P matrix properties given by Eq. (5), and there will be N identical natural frequencies. Since there is no structure coupling between the blades because of the rigid disk, the corresponding blade mode shapes for these N multiple frequencies can be any linearly independent combination of the blades [i.e., either the multiblade modes $\cos j\beta_r$ and $\sin j\beta_r$ given in Eq. (2), or simply $\alpha_j = 1$, and all other $\alpha_j = 0$]. If the mounting disks were flexible, then there would be coupling between the blades and the modes would resemble the $\cos j\beta_r$ and $\sin j\beta_r$ modes of Eq. (2), with each mode r having a slightly different frequency from another mode r.

For the mistuned rotor case, where, say, one blade had different mass and stiffness properties from all the others, Eq. (39) would now be all coupled together. In this case, the solution would give $N-1$ identical frequencies and one different one corresponding to the frequency of the mistuned blade. The blade mode shapes for the $N-1$ multiple frequencies would now show no participation of the mistuned blade but would otherwise be any linearly independent combination of the remaining equal blades, while the different frequency would show only the mistuned blade participating. For mounting on a flexible disk, all frequencies would then tend to be slightly different.

The above considerations for one mistuned blade can be extended to any number of mistuned blades on the rotor.

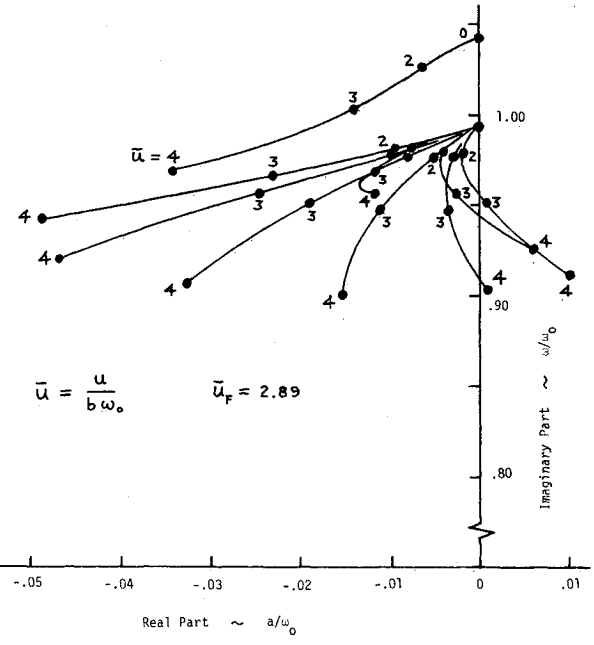

Fig. 5 Flutter root locus: blade 0 mistuned 5% in frequency. $N = 9$, $\xi = 45$ deg, $s/c = 1$, $\eta = 0.5$, $\nu_0 = 86.2$, $\zeta_j = 0$.

Application to Flutter Analysis

To investigate the torsional flutter of the rotor, one combines the standing wave representation of the rotor given by Eqs. (3) and (8) together with the standing wave representation of the air forces given by Eqs. (33-35) to obtain,

$$M\ddot{q} + C\dot{q} + Kq = 2\pi\rho U^2 b^2 P^T P\{B_2\sigma^2\ddot{q} + B_1\sigma\dot{q} + B_0 q + G_1 Y\} + P^T m_\alpha^D \tag{40}$$

$$\sigma\dot{Y}+g_0 Y=\sigma\dot{q} \tag{41}$$

where m_α^D represents an applied disturbance moment on the blades. All second, first, and zero derivative terms can then be combined to yield a series of linear differential equations whose stability can be examined by standard techniques. It is often convenient to nondimensionalize the above flutter equations by introducing a reference ω_0, a nondimensional time $\tau=\omega_0 t$, and the following nondimensional parameters,

$$\nu_j=I_{\alpha j}/\pi\rho b^4, \quad \tau=\omega_0 t, \quad \gamma_j=\omega_{\alpha j}/\omega_0$$

$$\bar{u}=\frac{U}{b\omega_0}, \quad \frac{\mathrm{d}}{\mathrm{d}\tau}=(\,\dot{}\,)=\frac{1}{\omega_0}\frac{\mathrm{d}}{\mathrm{d}t}, \quad m_\alpha^{D*}=\frac{m_\alpha^D}{\pi\rho b^4\omega_0^2} \tag{42}$$

Then, by noting that the blade stiffness and structural damping can be expressed as $k_{\alpha j}=I_{\alpha j}\omega_{\alpha j}^2$ and $C_j=2\zeta_j\omega_{\alpha j}I_{\alpha j}$, respectively, and dividing through by $\pi\rho b^4\omega_0^2$, one can rewrite Eqs. (40) and (41) in nondimensional form as,

$$M\ddot{q}+C\dot{q}+Kq+GY=P^T m_\alpha^{D*} \tag{43}$$

$$\dot{Y}+HY=\dot{q} \tag{44}$$

where the new, nondimensional matrices above are defined now as,

$$M=P^T[\ \nu_j\ ]P-2P^TPB_2$$

$$C=P^T[\ 2\zeta_j\gamma_j\nu_j\ ]P-2\bar{u}P^TPB_1$$

$$K=P^T[\ \nu_j\gamma_j^2\ ]P-2\bar{u}^2P^TPB_0$$

$$G=-2\bar{u}^2P^TPG_1, \qquad H=\bar{u}g_0 \tag{45}$$

The P^TP matrix appearing in the aerodynamic terms is a simple diagonal matrix equal to D as given by Eq. (5). For evaluation purposes, one recasts Eqs. (43) and (44) into first-order equations as,

$$L\dot{X}-NX=F \tag{46}$$

where one has,

$$L=\begin{bmatrix} I & 0 & 0 \\ 0 & M & 0 \\ 0 & 0 & I \end{bmatrix}, \quad N=\begin{bmatrix} 0 & I & 0 \\ -K & -C & -G \\ 0 & I & -H \end{bmatrix}$$

$$X=\begin{Bmatrix} q \\ \dot{q} \\ Y \end{Bmatrix}, \quad F=\begin{Bmatrix} 0 \\ P^T\ m_\alpha^{D*} \\ 0 \end{Bmatrix} \tag{47}$$

The overall matrices L,N,X,F now are of size $3N$, while the component matrices M,C,K, etc., are of size N. To look at the flutter problem, one sets $F=0$ in Eq. (46) and assumes solutions of the form

$$X=\bar{X}e^{pt}=\bar{X}e^{(p/\omega_0)\tau}$$

Placing this into Eq. (46) and multiplying through by the inverse of L results in the standard eigenvalue problem,

$$S\bar{X}=(p/\omega_0)\bar{X} \tag{49}$$

where,

$$S=\begin{bmatrix} 0 & I & 0 \\ -M^{-1}K & -M^{-1}C & -M^{-1}G \\ 0 & I & -H \end{bmatrix} \tag{50}$$

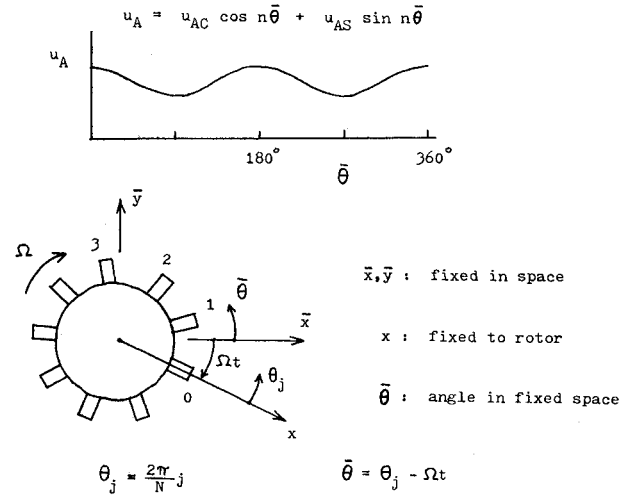

Fig. 6 Forced excitation of rotor.

One examines the roots, $p/\omega_0=a/\omega_0+i\omega/\omega_0$ of Eq. (49) as $\bar{u}$ increases. The presence of any roots with positive real parts indicates instability.

The above procedure was used to examine the flutter of the nine-bladed rotor ($N=9$) shown in Fig. 1, for both tuned and mistuned cases. The rotor and a stagger angle $\xi=45$ deg, a gap-to-chord ratio $s/c=1$, an inertia ratio $\nu_j=86.2$, the elastic axis at midchord $\eta=0.5$, and zero structural damping $\zeta_j=0$. See Fig. 1.

For the tuned case where all blades are equal, root loci of the pertinent nine roots p_j are shown plotted in Fig. 4 as the reduced velocity $\bar{u}=U/b\omega_0$ increases from zero. The critical velocity is $\bar{u}=2.43$ for the $r=1$ mode ($\beta_r=40$ deg), which coincides very well with that obtained from a standard traveling wave analysis. The roots p/ω_0, which here represent actual decay and amplification rates, seem to agree reasonably well with the damping margins g of traveling wave analyses. It should be noted that for these tuned cases, each mode r can be investigated independently here, since there is no coupling in the M, C, K, G, or H matrices between an r and an s mode. See Eqs. (45), (5), and (36).

For the mistuned case, one blade (blade *0*) was considered to be 5% higher in frequency than the remaining eight blades, due to some lesser mass. The corresponding root loci are shown plotted in Fig. 5 using the average frequency for the reference frequency ω_0 and average inertia for ν_0. No values of β_r are given, since the modes are all coupled together now. The critical velocity has now increased to $\bar{u}=2.89$ approximately. An examination of the resulting vibration patterns indicated low amplitude $\alpha_0=0.25$, $\alpha_1=0.15$, $\alpha_2=0.25$, then steadily rising values to a maximum of $\alpha_8=1$ at the last blade. Apparently the mistuning created a "dead spot" in the area of the mistuned blade and immediately after it.

A 5% "alternately" mistuned cascade was also studied and found to have an even greater critical velocity of $\bar{u}=3.92$ approximately. See Bundas[5] for further details. The mistuning effects here are similar in nature to those previously reported by Srinivasan[6] and Kaza and Kielb.[7]

Application of Forced Response

To investigate the forced response of a rotor, one goes back to Eqs. (40) and (41), or in nondimensional form, either Eqs. (43) and (44) or Eqs. (46) and (47). Two types of forcing disturbances $m_\alpha^D(t)$ will be considered, namely a periodic, engine order forcing of all the blades, and a transient, impulsive force on a single blade.

For the periodic, engine order forcing, one considers a steady but nonuniformly distributed airflow u_A passing

through the rotor. This aerodynamic distortion, which is caused by strut obstructions, local flow variations, etc., can be expressed as circumferential Fourier components for different radial locations. See Figs. 1 and 6. These velocity (and angle of attack) variations give rise to disturbance blade forces that also depend on the circumferential location of the blade. A particular Fourier component n of these blade forces can be expressed as,

$$m_{\alpha j}^{D^*} = f_{cn}\cos n\bar{\theta}_j + f_{sn}\sin n\bar{\theta}_j \tag{51}$$

where $m_{\alpha j}^{D^*}$ is the nondimensional disturbance moment defined by Eq. (43), f_{cn} and f_{sn} are appropriate nondimensional coefficients, and $\bar{\theta}_j$ represents the position of blade j with respect to axes fixed in space, as shown in Fig. 6. The position θ_j of the blade relative to the rotating rotor is related to the absolute position $\bar{\theta}_j$ by

$$\bar{\theta}_j = \theta_j - \Omega t \tag{52}$$

Placing Eq. (52) into Eq. (51) and expanding results in the blade moment

$$m_{\alpha j}^{D^*} = [f_{cn}\cos n\Omega t - f_{sn}\sin n\Omega t]\cos n\theta_j + [f_{cn}\sin n\Omega t + f_{sn}\cos n\Omega t]\sin n\theta_j \tag{53}$$

The above expression can be written more compactly using matrix form and complex harmonic notation as,

$$m_{\alpha}^{D^*} = T\begin{Bmatrix} 1 \\ -i \end{Bmatrix}\bar{f}_n e^{in\Omega t} \tag{54}$$

where,

$$T = \begin{bmatrix} \cos 0\frac{2\pi}{N}n & | & \sin 0\frac{2\pi}{N}n \\ \cos 1\frac{2\pi}{N}n & | & \sin 1\frac{2\pi}{N}n \\ \vdots & | & \vdots \\ \cos(N-1)\frac{2\pi}{N}n & | & \sin(N-1)\frac{2\pi}{N}n \end{bmatrix} \tag{55}$$

$$\bar{f}_n = f_{cn} + if_{sn} \tag{56}$$

and one takes the real part of Eq. (54) to obtain the physical Eq. (53). The response to the nth Fourier force components f_{cn} and f_{sn} in Eq. (51) are then obtained by placing Eq. (54) into Eqs. (46) and (47), assuming harmonic solutions of the form $X(t) = \bar{X}e^{in(\Omega/\omega_0)\tau}$, then solving for the complex amplitudes $\bar{X}$ from the complex algebraic equations,

$$\left[in\frac{\Omega}{\omega_0}L - N\right]\bar{X} = \begin{Bmatrix} 0 \\ P^T T\begin{Bmatrix} 1 \\ -i \end{Bmatrix} \\ 0 \end{Bmatrix}\bar{f}_n \tag{57}$$

Since $X = [q\ \dot{q}\ Y]^T$, the torsional response of any blade $\tilde{\alpha}_j$ is found by extracting the modal eigenvectors q from the X vector, then using the basic multiblade transformation equation (3) to obtain

$$\tilde{\alpha} = P\bar{q}e^{in\Omega t} \tag{58}$$

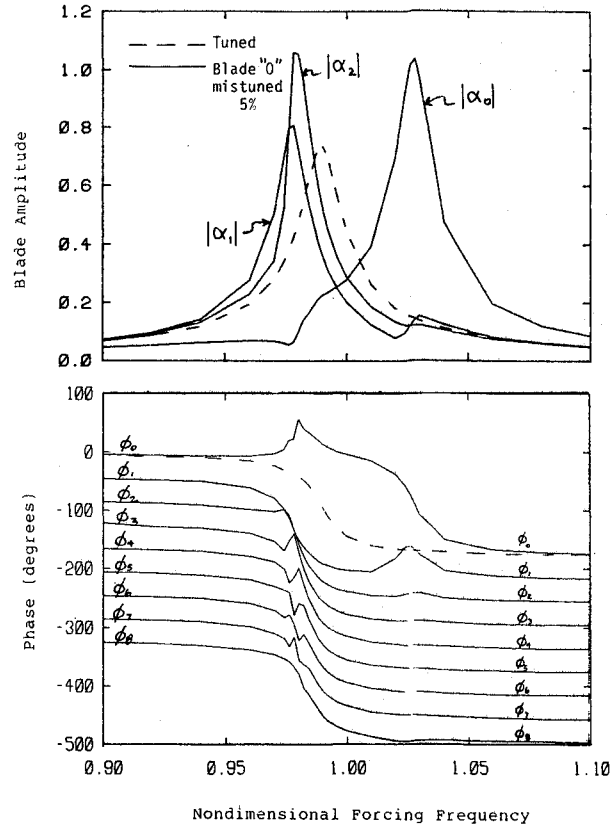

Fig. 7 Frequency response of tuned and mistuned rotor to $n=1$ engine order excitation.

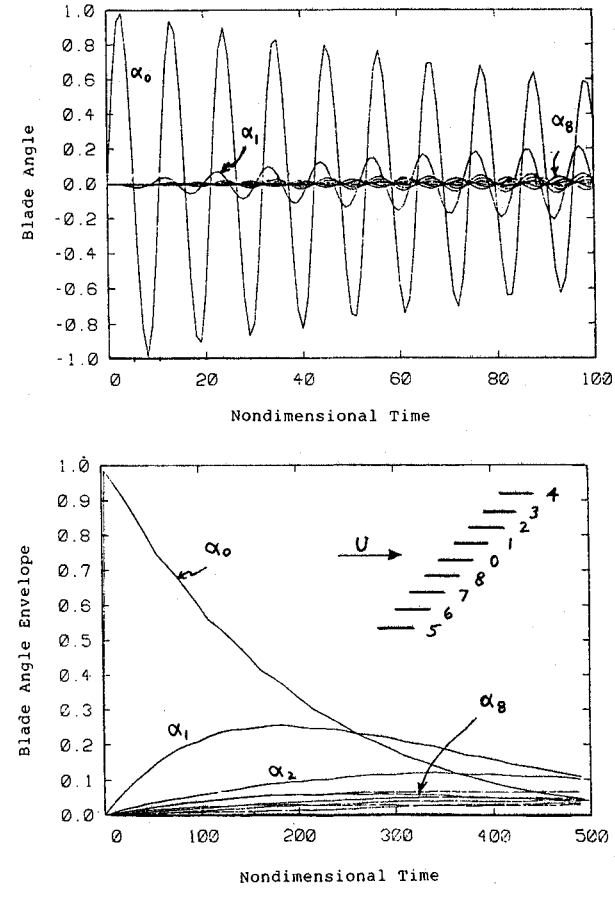

Fig. 8 Transient response of tuned cascade to impulsive loading of blade *0*.

Taking the real part of the above expression gives the response in the physical form, $\alpha(t) = \alpha_R \cos n\Omega t - \alpha_I \sin n\Omega t$ for any blade j.

In obtaining the engine order forcing, the matrix product $P^T T$ appearing in Eq. (57) plays a key role. Since the T matrix is simply 2 columns of the P matrix corresponding to a given mode n, the previous relations given by Eqs. (5) and (6) apply. Hence, an engine order Fourier harmonic n will give a direct F input into a mode r only if $n \pm r = 0, \pm N, \pm 2N, \ldots$. Thus, for a nine-bladed rotor $N=9$, the $r=0$ mode is excited directly only by $n=0,9,18,27,\ldots$, while the $r=2$ mode is excited directly by $n=2,7,11,16,20,\ldots$. The corresponding forcing frequency of these excitations is given from Eqs. (54) and (58) as $n\Omega$. Any natural frequencies of the rotor near $n\Omega$, particularly for a directly excited r mode, will cause resonances.

The previous analysis was used to examine the periodic engine order forcing response of a tuned and mistuned rotor. Figure 7 shows the blade amplitude and phase response of a nine-bladed rotor for engine order forcing $n=1$. For the tuned case, only the $r=1$ mode is excited and all the blades respond with equal amplitude $|\alpha_j|$ and with phase angle ϕ_j such that there is a constant interblade phase angle of 40 deg between them. The maximum amplitude is limited by the aerodynamic damping present in the air force coefficients. For the mistuned case where blade *0* was 5% higher in frequency, all the modes r of the rotor are now excited, and the individual blades now vibrate at different amplitudes. Generally, the forced response of the mistuned system is higher than for the tuned system. These same observations were found for the case of a 5% "alternately" mistuned cascade. See Bundas[5] for further details. Generally, these results are in agreement with those previously reported by Kaza and Kielb.[7]

In addition to the engine order forcing, the rotor was also excited by striking a single blade with a transient, impulsive force. This can be done simply by setting the disturbance moment for blade *0*, $m_{\alpha 0}^{D^*} = f(t)$, in Eqs. (47) and (46), integrating the resulting equations numerically to obtain q, then applying the basic multiblade transformation equation (3) to obtain the individual blade deflections α. For the case of a pure impluse moment, the problem can be alternatively formulated by setting all moments $m_{\alpha j}^{D^*} = 0$, applying velocity initial conditions $\alpha_j(0) = 0, \dot{\alpha}_0(0) = 1/I_0, \dot{\alpha}_1(0) = \dot{\alpha}_2(0) = \ldots = 0$, obtaining the corresponding initial conditions on q by inverting Eq. (3), then integrating as before. Figure 8 shows typical results for a tuned nine-bladed rotor struck by an impulse on blade *0*. The subsequent "ringing down" of the rotor was observed. Only the envelope of the response is shown in the lower half of Fig. 8. It should be noted that the only coupling between the blades for this rotor is through the aerodynamics. For a flexible disk rotor, more coupling between the blades would be experienced through the structural coupling.

With the standing wave analysis method described here, the response of a cascade to transient impacts can be studied, including the same aerodynamics as was used for the flutter analysis. The homogeneous solution of the equations gives the flutter characteristics, while the nonhomogeneous solution of the same equations gives the forced response, either to periodic engine order excitations or to transient impulsive forces.

Additional Comments

The present analysis dealt with a rotor whose blades were mounted on a rigid disk. In many rotors, the blades would be mounted on a flexible disk so that structural coupling between the blades would be present. To analyze these flexible disk rotors, one generally obtains the vibration modes of the coupled blade-disk system by a Rayleigh-Ritz or a finite element method, and then one expresses the torsion angle α at, say, the 80% blade span section in terms of a superposition of k normal coordinates $\xi(t)$ as,

$$\alpha = \Phi \xi \tag{59}$$

In the above, Φ is an $N \times k$ matrix relating the torsion angle α at each of the N blades for each of the k vibration modes assumed in the analysis. For tuned rotors, the vibration modes generally occur in pairs for each nodal diameter r, corresponding to the $\sin r\beta_j$ and $\cos r\beta_j$ modes used earlier for the rigid disk, Eq. (3). The standing wave analysis then expresses the rotor equations of motion in the uncoupled normal form as,

$$M\ddot{\xi} + 2\zeta_k \omega_k M\dot{\xi} + M\omega_k^2 \xi = \Xi \tag{60}$$

where the generalized force, $\Xi = \Phi^T m_\alpha$. To express the aerodynamic moments m_α of Eqs. (34) and (35) and the subsequent generalized force Ξ in terms of normal coordinates ξ, one notes that

$$\alpha = Pq = \Phi \xi \tag{61}$$

Multiplying by the inverse of P as given by Eq. (5) yields,

$$q = D^{-1} P^T \Phi \xi \tag{62}$$

which can be substituted into m_α and then into Ξ to obtain the generalized force,

$$\Xi = 2\pi\rho U^2 b^2 \{E_2 \sigma^2 \ddot{\xi} + E_1 \sigma \dot{\xi} + E_0 \xi + J_1 Y\} \tag{63}$$

$$\sigma \dot{Y} + g_0 Y = J_2 \sigma \dot{\xi} \tag{64}$$

where,

$$E_2 = \Phi^T P B_2 D^{-1} P^T \Phi, \qquad J_1 = \Phi^T P G_1$$

$$E_1 = \Phi^T P B_1 D^{-1} P^T \Phi, \qquad J_2 = D^{-1} P^T \Phi$$

$$E_0 = \Phi^T P B_0 D^{-1} P^T \Phi \tag{65}$$

and $\sigma = b/U$, while $B_2, B_1, B_0, G_1, g_0, Y$ are as defined in Eq. (36). Equations (63) and (64) can be readily incorporated into the flutter and forced vibration of tuned and mistuned flexible bladed-disk rotors, Eqs. (60) and (59).

For interest, it is sometimes useful to express the transient cascade aerodynamic influence coefficients, that is, how the motion of one blade α_j influences the forces on another blade $m_{\alpha i}$ in the cascade. This is readily done by inverting Eq. (3) to give,

$$q = D^{-1} P^T \alpha \tag{66}$$

then placing the above into the aerodynamic forces m_α of Eqs. (34) and (36) to give,

$$m_\alpha = 2\pi\rho U^2 b^2 \{E_2 \sigma^2 \ddot{\alpha} + E_1 \sigma \dot{\alpha} + E_0 \alpha + J_1 Y\} \tag{67}$$

$$\sigma \dot{Y} + g_0 Y = J_2 \sigma \dot{\alpha} \tag{68}$$

where the matrices E_2, E_1, E_0, J_1, J_2 are as defined in Eq. (65), but without the Φ or Φ^T matrices present. Keeping only α_0 and setting all other $\alpha_j = 0$ will give the moment on any other blade $m_{\alpha j}$ (including the blade *0*) due to motion of blade *0*, provided the number of blades N is large enough for cascade influence to die out.

Conclusions

The present article has given a unified standing wave approach to the flutter and forced response of turbine engine rotors. Both tuned and mistuned rotors can be readily accommodated.

The traditional traveling wave cascade air forces have been recast into standing wave arbitrary motion form, by making use of Padé approximants. Some standing wave coefficients are given for Whitehead's two-dimensional incompressible cascade theory.

Flutter analyses were conducted using standard constant coefficient, linear systems techniques. The analyses give true damping decay rates rather than damping margins. A typical example for a tuned and mistuned rotor is given.

The forced response of the rotor to periodic engine order excitation of all the blades, and to the transient impulsive excitation of a single blade is obtained using the same aerodynamic damping as for the flutter cases. Typical examples for a tuned and a mistuned rotor are given.

Extension of the procedure here is indicated for the case of flexible disk rotors, where structural as well as aerodynamic coupling exists between the blades. Also, the aerodynamic influence coefficients for the effect of one blade on the forces produced by another blade is given.

The standing wave analysis methods given here can be extended to other flow regimes by similar fitting of the sinusoidal traveling wave coefficients. Also they can be extended to flexible disk rotors as indicated previously. Because the equations are expressed completely in the time domain, these standing wave methods may prove to be more versatile for dealing with certain applications, such as coupling flutter with forced response and dynamic shaft problems, transient impulses on the rotor, low engine order excitation, bearing motions, and mistuning effects in rotors.

Acknowledgment

The authors wish to acknowledge helpful discussion with Prof. Edward Crawley, Kenneth Hall, and Dinkar Mokadam. Also, they wish to acknowledge the support of NASA Lewis Research Center, under NASA Grant No. NAG 3-214, Dr. R. Kielb, Technical Officer.

References

[1] Carta, F. O., "Coupled Blade-Disc-Shroud Flutter Instabilities in Turbojet Engine Rotors," *ASME Transactions, Journal of Engineering for Power*, Vol. 89, July 1967, pp. 419-426.

[2] Snyder, L. E. and Commerford, G. L., "Supersonic Unstalled Flutter in Fan Rotor: Analytic and Experimental Results," ASME Paper 74-GT-40, 1974.

[3] Mikolajczak, A. A., Arnoldi, R. A., Snyder, L. E., and Stargardter, H., "Advances in Fan and Compressor Blade Flutter Analysis and Predictions," *Journal of Aircraft*, Vol. 10, April 1975, pp. 325-332.

[4] Dugundji, J., "Flutter Analysis of a Tuned Rotor with Rigid and Flexible Disks," *MIT Gas Turbine and Plasma Dynamics Laboratory*, Cambridge, Mass., Rept. 146, July 1979.

[5] Bundas, D. J., "Flutter and Forced Response of Mistuned Rotors Using Standing Wave Analysis, S.M. Thesis, Dept. of Aeronautics and Astronautics, MIT, Cambridge, Mass., Jan. 1983; also, *MIT Gas Turbine and Plasma Dynamics Laboratory*, Rept. 170, March 1983.

[6] Srinivasan, A. V., "Influence of Mistuning on Blade Torsional Flutter," NASA CR-165137, Aug. 1980.

[7] Kaza, K. R. V. and Kielb, R. E., "Flutter and Response of a Mistuned Cascade in Incompressible Flow," *AIAA Journal*, Vol. 20, Aug. 1982, pp. 1120-1127.

[8] Hohenemser, K. H. and Yin, S. K., "Some Applications of the Methods of Multiblade Coordinates," *Journal of the American Helicopter Society*, Vol. 17, July 1972, pp. 3-12.

[9] Whitehead, D. S., "Force and Moment Coefficients for Vibrating Airfoils in Cascade," British Aeronautical Research Council, London, R.&M. 3254, Feb. 1960.

[10] Vepa, R., "On the Use of Padé Approximants to Represent Unsteady Aerodynamic Loads for Arbitrary Small Motions of Wings," AIAA Paper 76-17, 1976.

[11] Edwards, J. W., Ashley, H., and Breakwell, J. V., "Unsteady Aerodynamic Modeling for Arbitrary Motions," *AIAA Journal*, Vol. 17, April 1979, pp. 365-374.

[12] Bisplinghoff, R. L., Ashley, H., and Halfman, R. L., *Aeroelasticity*, Addison-Wesley Publishing Co., Cambridge, Mass., 1955.

[13] Rock, S. M. and DeBra, D. B., "Prediction and Experimental Verification of Transient Airfoil Motion, *Journal of Aircraft*, Vol. 19, June 1982, pp. 456-464.